Journal of Magnetic Resonance 301 (2019) 94–101

Contents lists available at ScienceDirect

Journal of Magnetic Resonance

journal homepage: www.elsevier.com/locate/jmr

# A greedy variational approach for generating sparse $T_1$-$T_2$ NMR relaxation time distributions

Can Evren Yarman *, Jonathan Mitchell

*Schlumberger Cambridge Research, High Cross, Madingley Road, Cambridge CB3 0EL, UK*

ARTICLE INFO

*Article history:*
Received 2 January 2019
Revised 27 February 2019
Accepted 28 February 2019
Available online 1 March 2019

*Keywords:*
Greedy algorithm
$T_1$-$T_2$
Discrete component fit
Inverse method

ABSTRACT

We present a nonlinear inversion method for generating sparse solutions to the Fredholm Integral equation describing two-dimensional distributions of nuclear magnetic resonance (NMR) relaxation times or diffusion coefficients. Our greedy variational method approximates the distribution of exponential rate constants using a sum of Dirac delta functions, which constitute our dictionary elements. The greedy nature of the method promotes sparsity in the representation by iteratively increasing the number of terms. The variational component estimates the parameters of the Dirac delta functions from a continuum at each iteration by reducing the least squares misfit to the data. Unlike sparsity promoting linearized inversion methods, where the dictionary is fixed and can exponentially grow in the case of multiple variables or when searching for higher resolution, the greedy component of our method aims to keep the dictionary small while the variational component keeps the dictionary dynamic. We demonstrate our method with synthetic data and experimental measurements of $T_1$-$T_2$ correlations of liquid-saturated porous rocks. The sparsity of the approximate solutions is ideal for real-time processing and transmission in remote or mobile NMR applications such as well logging.



## 1. Introduction

Multi-dimensional correlations of nuclear magnetic resonance (NMR) relaxation times (longitudinal $T_1$ and transverse $T_2$) or diffusion coefficients $D$ provide a powerful method for characterizing complex materials such as liquid-saturated porous media. The data are often described by an unknown number of exponential rate constants and interpretation can be complicated by the coupling of eigenfunctions describing the different relaxation or diffusion processes represented by the experimental dimensions [1]. A popular method for visualizing the results is numerical inversion based on Tikhonov regularization [2] that provides an approximate solution to the first kind Fredholm integral equation modeling the data [3]. Methods for generating these smooth, bounded distributions are established in the NMR community and widely used in a number of industries [4–6]. In particular, the oil and gas industry routinely measures NMR distributions of $T_2$ [7], $T_1$-$T_2$ [8], and $D$-$T_2$ [9] in down-hole well logs and laboratory core analysis to identify hydrocarbon resources. The integrals of these distributions provide key petrophysical parameters, such as fluid-phase discrimination, irreducible water saturation, porosity, and permeability [10,11].

Despite the prevalence of regularization methods for producing smooth, pseudo-continuous distributions of relaxation time or diffusion coefficients, it is not obvious that this representation is physically meaningful. The argument for a continuous distribution of relaxation times follows from the work of Brownstein and Tarr [12]. In an isolated one-dimensional pore (slot) governed by "fast diffusion" the relaxation process is described by a single eigenfunction-eigenvalue pair (where the eigenvalue is the relaxation rate) determined by the pore geometry. If many isolated pores are present with a distribution of sizes, there will be corresponding distribution of eigenvalues and hence a distribution of relaxation rates. However, when the pores are connected (as in most physical porous media), the eigenfunctions extend across all space (although their amplitude may be spatially dependent [13]) and so the sample could be characterized by a few eigenfunction-eigenvalue pairs or many eigenfunctions with similar eigenvalues. Unfortunately, this inverse problem is ill-conditioned so there is insufficient information in the data to differentiate between these solutions.

Practically, one may have a good reason for preferring a sparse solution. For example, in real-time logging-while-drilling (LWD) applications there is limited bandwidth for transmission of data from the down-hole tool to the surface. Data compression is required and a sparse dictionary of relaxation rates and amplitudes

* Corresponding author.
*E-mail address:* CYarman@slb.com (C.E. Yarman).

https://doi.org/10.1016/j.jmr.2019.02.009
1090-7807/

that provides an approximate representation of the data is an efficient option. The latest generation of LWD NMR tools are capable of measuring $T_1$-$T_2$ relaxation time correlations [14], considered essential for the characterization of unconventional organic shale reservoirs [15]. Accordingly, we have developed a method for generating a minimal sparse representation which we demonstrate using synthetic data and laboratory measurements of $T_1$-$T_2$ correlations in a selection of brine-saturated rocks. The NMR experiment comprises an inversion-recovery pulse sequence [16] to encode $T_1$, followed by a Carr-Purcell-Meiboom-Gill (CPMG) pulse sequence [17,18] to encode $T_2$. The longitudinal recovery delay $\tau_1$ and the transverse decay time $\tau_2$ are varied independently. We denote the acquired data (magnetization) by the multivariate function $M(\tau_1,\tau_2)$ which comprises signal $S(\tau_1,\tau_2)$ plus noise $E(\tau_1,\tau_2)$,

$$M(\tau_1,\tau_2) = S(\tau_1,\tau_2) + E(\tau_1,\tau_2). \tag{1}$$

The NMR relaxation times are described by the distribution $f(T_1,T_2)$ and relate to the signal via the Fredholm integral equation

$$S(\tau_1,\tau_2) = \int_{\mathbb{R}_+\times\mathbb{R}_+} \left(1-2\exp\left\{-\frac{\tau_1}{T_1}\right\}\right)\exp\left\{-\frac{\tau_2}{T_2}\right\} f(T_1,T_2)\mathrm{d}T_1\mathrm{d}T_2. \tag{2}$$

Current inversion approaches are dominated by linear methods [19,3,20,21] which consider a discrete approximation of the integral for a fixed chosen set of relaxation times $(T_{1,m},T_{2,m})_{m=1}^N$ and integration weights $w_m$,

$$M(\tau_1,\tau_2) = \sum_{m=1}^{N} w_m f(T_{1,m},T_{2,m})\left(1-2\exp\left\{-\frac{\tau_1}{T_{1,m}}\right\}\right)\exp\left\{-\frac{\tau_2}{T_{2,m}}\right\} + E(\tau_1,\tau_2), \tag{3}$$

and compute $f(T_{1,m},T_{2,m})$ by solving a linear system using the measurements made at $(\tau_{1,k},\tau_{2,k})_{k=1}^K$. Depending on the discretization of the $(\tau_1,\tau_2)\times(T_1,T_2)$ space, the linear problem, which requires inversion of the kernel matrix $A_{km} = \left(1-2\exp\left\{-\frac{\tau_{1,k}}{T_{1,m}}\right\}\right)\exp\left\{-\frac{\tau_{2,k}}{T_{2,m}}\right\}$, can be severely ill-posed [3]. Regularization strategies, such as imposing smoothness, sparsity, or Bayesian priors on some approximate representation of $f(T_{1,m},T_{2,m})$, are required to stabilize the inversion. A common approximate representation of $f(T_1,T_2)$ is a superposition of functions, such as those from an over complete dictionary [22,14]

$$f(T_1,T_2) \approx \sum_m a_m b_m(T_1-T_{1,m},T_2-T_{2,m}), \tag{4}$$

where $a$ is the amplitude, for some absolutely integrable functions $b_m(T_1,T_2)$ or discrete measurements [23] such that

$$f(T_1,T_2) \approx \sum_m a_m \delta(T_1-T_{1,m})\delta(T_2-T_{2,m}), \tag{5}$$

where $\delta(t)$ is the Dirac delta function. Eq. (5) can be regarded a special case of Eq. (4) because any absolutely integrable function can be used to approximate the Dirac delta function.[1] It should be noted that the choice of representation does not aim to eliminate the ill-posed nature of the inversion problem, but enforce regularization in a domain of choice. For $a_m = w_m f(T_{1,m},T_{2,m})$, substitution of Eq. (5) into Eq. (2) leads to Eq. (3).

In this work, we assume $f(T_1,T_2)$ is in the form of Eq. (5). Unlike the linear approaches used previously, we do not assume a fixed set of relaxation times. Instead we construct data dependent numerical quadratures to approximate the integral in Eq. (1). Thus, the NMR inversion problem considers a discrete approximation of the integral in Eq. (1) according to

$$M(\tau_1,\tau_2) = \sum_{m=1}^{N} a_m\left(1-2\exp\left\{-\frac{\tau_1}{T_{1,m}}\right\}\right)\exp\left\{-\frac{\tau_2}{T_{2,m}}\right\} + E(\tau_1,\tau_2), \tag{6}$$

for some unknown $N \geqslant 1$, and aims to determine a set of (positive) parameters $(a_m,T_{1,m},T_{2,m})$ such that $E(\tau_1,\tau_2)$ is within a desired tolerance.

We propose a greedy variational approach to address the inversion problem. Our method is a nonlinear inversion in the spirit of multivariate continuous pursuit methods [24] with the difference that instead of basis pursuit, our approach could be considered as a continuous variant of orthogonal matching pursuit. Compared to Monte Carlo based non-linear optimization methods [25,26], which could be characterized as global random search strategies for finding a solution, our method performs a structured descent type search. Descent type methods are appealing because the computational cost of these methods is proportional to the number of elements utilized to represent the data [27,28,24]. Compared to the semi-analytic method in [23], which requires uniform sampling of $\tau_2$, our method works with non-uniformly sampled $\tau_{1,k}$ and $\tau_{2,k}$ and provides a simultaneous inversion of both data dimensions rather than a sequential inversion. Non-uniform sampling of $\tau_{1,k}$ is common, and non-uniform sampling of $\tau_{2,k}$ could be of interest for optimized data acquisition protocols.

The outline of our paper is as follows. The computational and experimental methods are described in Sections 2 and 5, respectively. The computational methods is demonstrated in application to synthetic and experimental data in Section 3. Finally, we conclude our discussion in Section 4.

## 2. Computational method

We employ a greedy approach to the inversion problem where we iteratively increase the number of terms in the sum by one until the error is below a desired threshold. At every iteration we optimize the parameters of previous, as well as newly introduced terms, to minimize a cost function using a variational approach. In our study we minimized weighted least square error (see Eq. (8)). Note that this is a global norm that doesn't necessarily guarantee that residual is normally distributed.

Let $P_n = \{(a_m,T_{1,m},T_{2,m})_{m=1}^n\}$ be the set of $n$ parameters and $R_n(\tau_1,\tau_2;P_n)$ denote the corresponding data misfit residual defined by

$$R_n(\tau_1,\tau_2;P_n) = M(\tau_1,\tau_2) - \sum_{m=1}^{n} a_m\left(1-2\exp\left\{-\frac{\tau_1}{T_{1,m}}\right\}\right)\exp\left\{-\frac{\tau_2}{T_{2,m}}\right\}, \tag{7}$$

for $n>0$. The weighted least squares error is defined as

$$J_n(P_n) = \frac{1}{2}\sum_{k=1}^{K} w_k\left[R_n(\tau_{1,k},\tau_{2,k};P_n)\right]^2, \tag{8}$$

for some positive weight $w_k$ and samples $(\tau_{1,k},\tau_{2,k})_{k=1}^K$. We define $P_{n,1}$ to be the set of $\{(a_m,T_{1,m},T_{2,m})_{m=1}^n\}$ that (locally) minimizes $J_n$:

$$P_{n,1} = \arg\min_{\{(a_m,T_{1,m},T_{2,m})_{m=1}^n\}} J_n\left(\{(a_m,T_{1,m},T_{2,m})_{m=1}^n\}\right). \tag{9}$$

We minimize $J_n$ using a variational method which requires an initial guess. We initialize the variational method with $P_{n,0} = P_{n-1,1}\cup P_{1,n}$ where $P_{1,n}$ minimizes the least squares error to the residual at the $(n-1)^{\text{th}}$ iteration:

[1] Let $f(t)$ be an absolutely integrable function, i.e. $\int|f(t)|dt<\infty$, then $\delta(t) = \lim_{\sigma\to\infty}\frac{f(\sigma^{-1}t)}{\int|f(\sigma^{-1}t)|\mathrm{d}t}$.

**Table 1**
Parameters $(a_m, T_{1,m}, T_{2,m})$ used to generate synthetic $T_1$-$T_2$ data and the corresponding fitted results without noise (SNR $= \infty$) and with added Gaussian noise (SNR $\approx 15$). The parameters are ordered in ascending values of $T_{1,m}$; assignment of index $m$ is arbitrary in the fit. The relaxation time ratios are also given in the table. The synthetic data and fits are shown in Fig. 1.

| $m$ | $a_m$ | $T_{1,m}$/s | $T_{2,m}$/s | $T_1/T_2$ |
|---|---|---|---|---|
| | | Synthetic parameters | | |
| 1 | 0.2768 | 0.0280 | 0.0224 | 1.25 |
| 2 | 0.2774 | 0.0324 | 0.0259 | 1.25 |
| 3 | 0.2633 | 0.0375 | 0.0300 | 1.25 |
| 4 | 0.0074 | 2.3178 | 1.1589 | 2.00 |
| 5 | 0.1751 | 2.6826 | 1.3413 | 2.00 |
| | | Fit parameters (SNR $= \infty$) | | |
| 1 | 0.6892 | 0.0303 | 0.0247 | 1.23 |
| 2 | 0.1280 | 0.0456 | 0.0335 | 1.36 |
| 3 | 0.0004 | 0.0494 | 0.0381 | 1.30 |
| 4 | 0.1824 | 2.6676 | 1.3348 | 2.00 |
| | | Fit parameters (SNR $\approx 15$) | | |
| 1 | 0.7200 | 0.0315 | 0.0251 | 1.25 |
| 2 | 0.0998 | 0.0583 | 0.0318 | 1.83 |
| 3 | 0.1802 | 2.7164 | 1.3834 | 1.97 |

$$P_{1,n} = \arg \min_{(a,T_1,T_2)} J_{n,0}(a, T_1, T_2), \tag{10}$$

with

$$J_{n,0}(a, T_1, T_2) = \frac{1}{2} \sum w_k \left[ R_{n-1}(\tau_{1,k}, \tau_{2,k}; P_{n-1,1}) - a\left(1 - 2\exp\left\{-\frac{\tau_{1,k}}{T_1}\right\}\right)\exp\left\{-\frac{\tau_{2,k}}{T_2}\right\}\right]^2. \tag{11}$$

We define $P_{0,1} = \varnothing$ to be the empty set, making $P_{1,0} = P_{1,1}$.

### 2.1. Choice of weights

The measured NMR data are described by real and quadrature (imaginary) channels. The data are phase rotated to maximize $M(\tau_1, \tau_2)$ in the real channel. An estimate of the noise $E(\tau_1, \tau_2)$ in Eq. (1) is then obtained from the quadrature channel. Inspection of experimental data indicates that the noise is approximately normally distributed [29] with zero mean and variance $\sigma^2(\tau_1), E(\tau_1, \tau_2) \in \mathcal{N}(0, \sigma^2(\tau_1))$. Consequently, we see that $R_n$ in Eq. (7) is an estimate of the noise. In the context of Bayesian inversion, each term of $J_n$ is related to the logarithm of the probability

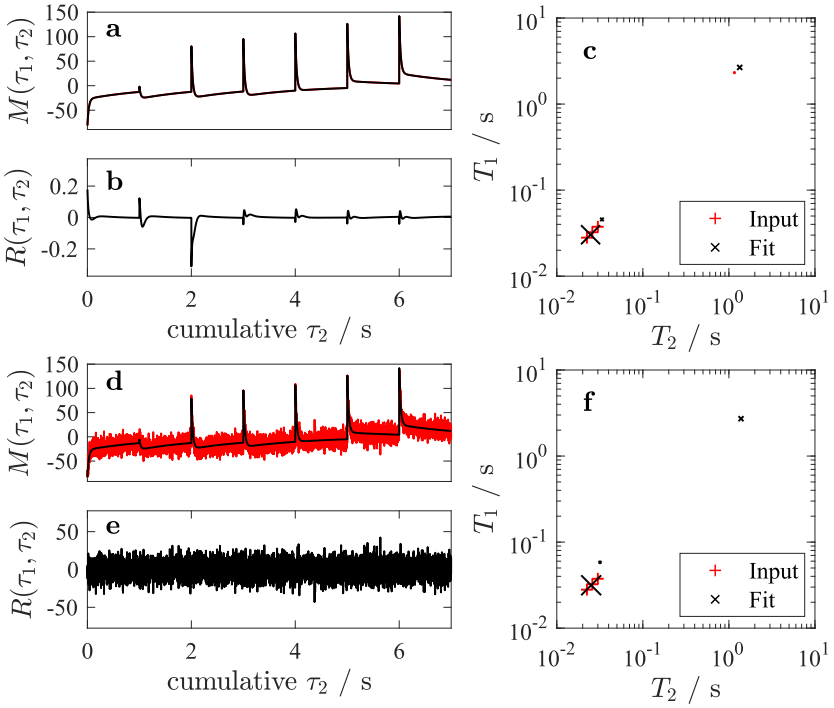


**Fig. 1.** Greedy variational algorithm fit to noise-free synthetic $T_1$-$T_2$ data (a-c). The synthetic data are shown in (a, red line) with the corresponding fit overlaid (a, black line); the data and fit are indistinguishable in this plot. The fit residuals are given in (b). The parameter sets $(a_m, T_{1,m}, T_{2,m})$ are plotted in (c) where the marker size is proportional to $a_m$. The algorithm was applied to the same synthetic data with added noise (d-f). The noisy data are shown in (d, red line) with the corresponding fit overlaid (d, black line). The residuals are shown in (e) with the parameter sets $(a_m, T_{1,m}, T_{2,m})$ plotted in (f) where the marker size is proportional to $a_m$. The parameter set values are listed in Table 1. (For interpretation of the references to colour in this figure legend, the reader is referred to the web version of this article.)

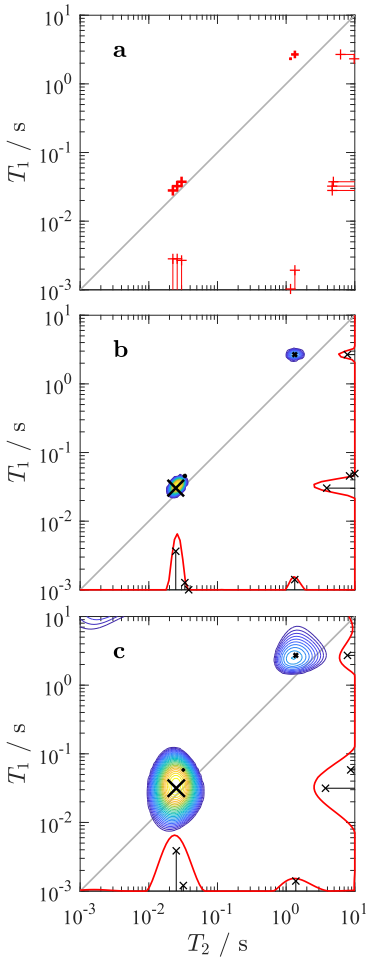


**Fig. 2.** Tikhonov regularization applied to synthetic $T_1$-$T_2$ data. The synthetic parameter set $(a_m, T_{1,m}, T_{2,m})$ is shown in (a) for reference: red + symbols where the marker size proportional to $a_m$, repeated from Fig. 1 and Table 1. Marginal projections (stem plots) are included for clarity. The pseudo-continuous $T_1$-$T_2$ distribution generated from the noise-free synthetic data is shown in (b, contours) with marginal projections (red lines) included for clarity. The fitted parameter set $(a_m, T_{1,m}, T_{2,m})$ from Table 1 is overlaid: black × symbols in the main plot (marker size is proportional to $a_m$) and stems in the marginal projections. The pseudo-continuous $T_1$-$T_2$ distribution generated from the noisy synthetic data is shown in (c, contours) with marginal projections (red lines) included for clarity. The fitted parameter set $(a_m, T_{1,m}, T_{2,m})$ from Table 1 is overlaid: black × symbols in the main plot (marker size is proportional to $a_m$) and stems in the marginal projections. In each plot the diagonal gray line indicates $T_1 = T_2$. (For interpretation of the references to colour in this figure legend, the reader is referred to the web version of this article.)

distribution of noise which is a Gaussian. Consequently, the choice for the weights in Eq. (8) becomes one over the variance of the noise, which we approximate by

$$w_k^{-1} = \sigma^2(\tau_{1,k}) \approx \frac{\sum_{l=1}^{L}\left[E(\tau_{1,k},\tau_{2,l})\right]^2}{\sum_{l=1}^{L} 1}, \tag{12}$$

where $L$ is the number of $\tau_2$ samples for a given $\tau_{1,k}$.

### 2.2. Estimation of $P_{1,n}$

The weighted least squares error $J_{n,0}(a, T_1, T_2)$ is non-linear in $(T_1, T_2)$. Therefore we use a variational approach to (locally) minimize $J_{n,0}(a, T_1, T_2)$ which is initialized by choosing the minimizer of a fixed set $\mathcal{T}_{1,2}$ of a few $(T_1, T_2)$ values:

$$P_{0,n} = \underset{\substack{(a,T_1,T_2)\\(T_1,T_2)\in\mathcal{T}_{1,2}}}{\arg\min} J_{n,0}(a, T_1, T_2) \tag{13}$$

In our implementation we choose

$$\mathcal{T}_{1,2} = \left\{(T_1,T_2) | T_1 = T_2 = 10^k, k = -5,-4,\ldots,-1,0,1,\ldots,4,5\right\}.$$

Note that for fixed $(T_1, T_2)$, computation of $a$ is a quadratic minimization problem with the solution

$$a(T_1,T_2) = \frac{\sum_k w_k R_{n-1}(\tau_{1,k},\tau_{2,k};P_{n-1,1})\left(1-2\exp\left\{-\frac{\tau_{1,k}}{T_1}\right\}\right)\exp\left\{-\frac{\tau_{2,k}}{T_2}\right\}}{\sum_k w_k\left[\left(1-2\exp\left\{-\frac{\tau_{1,k}}{T_1}\right\}\right)\exp\left\{-\frac{\tau_{2,k}}{T_2}\right\}\right]^2}. \tag{14}$$

Thus $P_{0,n}$ is found from $J_{n,0}(a, T_1, T_2)$ evaluated at the values $(a, T_1, T_2) \in \{(a(T_1, T_2), T_1, T_2) | (T_1, T_2) \in \mathcal{T}_{1,2}\}$.

### 2.3. Stopping criteria

Let $\mathbb{E}$ denote the expectation of a random variable. Recall that $R_n$ is an estimate of the noise at the $n^{\text{th}}$ iteration. As $n$ increases, we expect $R_n$ to converge to $E$. Consequently, Eq. (14), in expectation, should converge to

$$\begin{aligned}\mathbb{E}\left[\frac{\sum_k w_k E(\tau_{1,k},\tau_{2,k})\left(1-2\exp\left\{-\frac{\tau_{1,k}}{T_1}\right\}\right)\exp\left\{-\frac{\tau_{2,k}}{T_2}\right\}}{\sum_k w_k\left[\left(1-2\exp\left\{-\frac{\tau_{1,k}}{T_1}\right\}\right)\exp\left\{-\frac{\tau_{2,k}}{T_2}\right\}\right]^2}\right]\\ \approx \frac{\sum_k \mathbb{E}\left[E(\tau_{1,k},\tau_{2,k})\right] w_k\left(1-2\exp\left\{-\frac{\tau_{1,k}}{T_1}\right\}\right)\exp\left\{-\frac{\tau_{2,k}}{T_2}\right\}}{\sum_k w_k\left[\left(1-2\exp\left\{-\frac{\tau_{1,k}}{T_1}\right\}\right)\exp\left\{-\frac{\tau_{2,k}}{T_2}\right\}\right]^2},\end{aligned} \tag{15}$$

which, by $E(\tau_1, \tau_2) \in \mathcal{N}(0, \sigma^2(\tau_1))$, is zero. In light of this outcome, when the amplitude $a$ of $P_{0,n}$ is approximately zero, which for practical purposes is chosen as some small threshold, we stop iterating the terms in the summation of Eq. (6).

**Algorithm 1.** $T_1$-$T_2$ inversion

1. Set $n = 1$.
   (a) Discrete search for a single basis element. Compute $P_{1,0} \in \mathcal{T}_{1,2}$ that minimizes $J_{1,0}$.
   (b) Dynamic search for a single basis element. Compute $P_{1,1}$ that minimizes $J_{1,0}$ around $P_{1,0}$.
2. Set $n = 2$
   (a) Discrete search for a single basis element. Compute $P_{n,0} \in \mathcal{T}_{1,2}$ that minimizes $J_{n,0}$.
   (b) Check if the error criterion is satisfied which in our case is weighted least square error. If the error criterion isn't satisfied, continue. Stop otherwise.
   (c) Dynamic search for a single basis element. Compute $P_{1,n}$ that minimizes $J_{n,0}$ around $P_{n,0}$.
   (d) Dynamic search for all basis elements. Compute $P_{n,1}$ that minimizes $J_n$ around $P_{n-1} \cup P_{1,n}$.
   (e) Set $n$ to $n + 1$ and go to step 2a.

### 2.4. The algorithm

We summarize the proposed method in Algorithm 1. The computational complexity of this algorithm increases iteratively as $n$ increases. Steps 1a and 2a have a fixed computational cost which consists of a fixed number $|\mathcal{T}_{1,2}|$ of evaluations of $J_{1,0}$ to minimize the evaluated values. Consequently, step 2b is a single logical operation to check whether the estimated linear parameters $a_m$ are below the chosen threshold. The computational complexity is

**Table 2**
Parameters $(a_m, T_{1,m}, T_{2,m})$ obtained by fitting experimental $T_1$-$T_2$ data acquired for a selection of samples. The parameters are ordered in descending values of $a_m$; assignment of index $m$ is arbitrary in the fit. The relaxation time ratios are also given in the table. The data and fits are shown in Fig. 3.

| $m$ | $a_m$ | $T_{1,m}$/s | $T_{2,m}$/s | $T_1/T_2$ |
|---|---|---|---|---|
| | | Doped water | | |
| 1 | 0.989 | 0.064 | 0.064 | 1.00 |
| 2 | 0.011 | 0.001 | 0.023 | 0.03 |
| | | Ohio Blue sandstone | | |
| 1 | 0.774 | 0.037 | 0.013 | 2.85 |
| 2 | 0.226 | 0.185 | 0.064 | 2.89 |
| | | Ketton limestone | | |
| 1 | 0.382 | 0.019 | 0.013 | 1.46 |
| 2 | 0.242 | 0.147 | 0.096 | 1.53 |
| 3 | 0.236 | 0.440 | 0.398 | 1.11 |
| 4 | 0.117 | 1.540 | 1.169 | 1.32 |
| 5 | 0.019 | 0.093 | 0.367 | 0.25 |
| 6 | 0.004 | 1.467 | 5.265 | 0.28 |
| | | Shale | | |
| 1 | 0.748 | $T_1$ | 0.001 | 2.90 |
| 2 | 0.142 | 0.057 | 0.032 | 1.78 |
| 3 | 0.110 | 0.489 | 0.391 | 1.25 |

dominated by the optimization steps used for the dynamic search. In our implementation of steps 1b and 2c, we use a descent type dynamic search for a single atom. We use the BFGS algorithm [30], a gradient-based optimization method, on the tree variables $(a, T_1, T_2)$ of a single element of the dictionary. Similarly, step 2b utilizes BFGS on the $\{(a_m, T_{1,m}, T_{2,m})\}_{m=1}^{n}, 3n$ variables. The computational complexity of the algorithm is dominated by this step as $n$ increases. The convergence rate could be improved using variable projection [31] on the linear parameters $a_m$, for example. Our main objective here is to demonstrate the feasibility of the proposed method for the inversion of NMR data. We will investigate the performance of other initialization and optimization methods in a future study.

## 3. Results

### 3.1. Synthetic data

We applied the proposed method on noise-free synthetic data generated using the parameter set $(a_m, T_{1,m}, T_{2,m})$ in Table 1. We define the signal-to-noise ratio (SNR) by maximum signal divided by the root mean square of the noise in quadrature channel. Thus the SNR of noise-free synthetic data was infinite, which is to say $\epsilon_n(k) = 0$ for all $n, k$, and the simulated acquisition parameters $(t_e, t_{W,n}, K_n)$ were $(\tau_{1,k}, \tau_{2,k}) \in \{(t_{W,n}, q) | n = 1, \ldots, 7, q = t_e, \ldots, K_n t_e\}$ with $t_e = 1$ ms and $K_n = K = 1000$. A challenging parameter set with $m = 1 \ldots 5$ was selected to test the algorithm, consisting of two groups of closely-spaced relaxation times. The synthetic data are plotted in Fig. 1(a) with the data rows stacked in order of increasing $t_W$ on a cumulative acquisition time abscissa equivalent to $\sum_{n=1}^{7} n\tau_2$. The recovered $T_1$-$T_2$ distribution is shown in (c) (also Fig. 2(a)). In the absence of noise, the algorithm provides a very close approximation to the synthetic data with negligible fit residuals, see Fig. 1(b). However, the algorithm only returns 4 components rather than the expected 5, see Table 1. As can be seen in the $T_1$-$T_2$ plot, Fig. 1(c), the algorithm has represented several components with a single, large amplitude component. This outcome is entirely reasonable and expected as the algorithm is designed to minimize the number of components required to fit the data within the specified tolerance. For comparison, it is interesting to note that the smoothed regularization technique used to generate pseudo-continuous $T_1$-$T_2$ distributions fails to distinguish between the closely-spaced components and returns just two peaks, see Fig. 2(b). Note that the scaling of the marginal projections in Fig. 2 has been chosen arbitrarily to allow the continuous distributions (red solid lines) and discrete components (stems) to be shown on the same axes.

When significant noise is added to the synthetic data, Fig. 1(d) with SNR $\approx 15$, the algorithm continues to perform reliably. This time only 3 components are identified, see Table 1, but the fit residuals are consistent with Gaussian-like noise in Fig. 1(e) and the main clusters of components are captured in Fig. 1(f). Our algorithm is extremely robust to noise, whereas the Tikhonov regularization approach massively broadens the pseudo-continuous $T_1$-$T_2$ distribution to compensate, see Fig. 2(c). Overall, our algorithm and the Tikhonov regularization approach of [3] provide the consistent solutions.

### 3.2. Experimental data

We applied our algorithm to experimental $T_1$-$T_2$ correlation data acquired from liquid-saturated rock samples. As the measurements were performed at low field, a ratio $T_1/T_2 \sim 2$ was expected always [32]. Samples of doped water, Ohio Blue sandstone, Ketton limestone, and organic shale were measured. The fitted parameters are listed in Table 2. For doped water, a single dominant component was present as expected. A secondary component of negligible amplitude was also returned by the algorithm. From an interpretation point of view, those components can be treated as unphysical since $T_1/T_2 \ll 1$. Similarly, for the Ketton limestone, the fitted low-amplitude components $m = 5, 6$ with $T_1/T_2 < 1$ can be considered artifacts. These components can be rejected in postprocessing for interpretation purposes. Alternatively, constraints can be incorporated in the inversion. We did not include such constraints here to avoid biasing the results towards a particular outcome.

The fit quality achieved with the greedy variational algorithm is illustrated in Fig. 3 for the experimental data. For the doped water, the residuals in Fig. 3(b) appear as Gaussian-distributed noise. For the liquid-saturated rock samples, larger residuals are observed relative to $M(\tau_1, \tau_2)$. The large-amplitude spikes in the residual plots, notable in Fig. 3(e,h), correspond to the first few echoes in each CPMG train. A non-exponential decay can be observed in these early data due to imperfect rf pulses and magnetic field

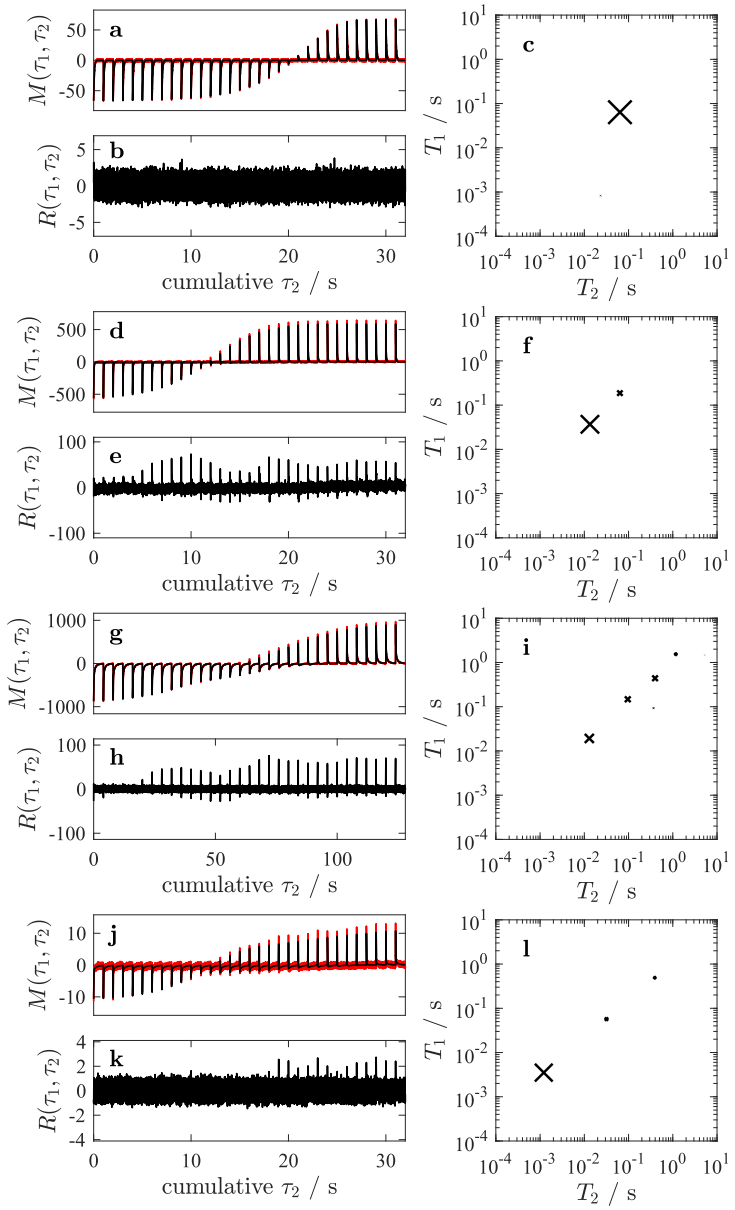


**Fig. 3.** Greedy variational algorithm applied to experiment NMR $T_1$-$T_2$ data acquired for a selection of samples. Results are presented for (a-c) doped water, (d-f) Ohio Blue sandstone, (g-i) Ketton limestone, and (j-k) an organic shale. For each sample, the raw data are shown in the first plot (solid red line) with the fit overlaid (solid black line), the fit residuals are shown in the second plot, and the fitted discrete $T_1$-$T_2$ components in the third plot ($\times$ symbols, where the marker size is proportional to $a_m$). (For interpretation of the references to colour in this figure legend, the reader is referred to the web version of this article.)

inhomogeneities [33], and so the inability of the algorithm to capture the short-time behavior is unsurprising. The fit quality could be improved by increasing the number of terms, but the algorithm has selected the minimum number required to meet the specified tolerance in each case.

For the experimental data, we do not know *a priori* the underlying relaxation time distribution. Therefore, we compare the fitted parameter sets $(a_m, T_{1,m}, T_{2,m})$ to conventional pseudo-continuous $T_1$-$T_2$ distribution generated by Tikhonov regularization. The $T_1$-$T_2$ distribution plots are given in Fig. 4 for the selection of experimental samples. The greedy variational algorithm components have been overlaid. Again, the scaling of the marginal projections has been chosen arbitrarily to allow the pseudo-continuous distributions (red solid lines) and discrete components (stems) to be represented on the same axes. In all cases, there is good agreement between the two solutions. The discrete component amplitudes $a_m$ are equivalent to the integrals of the corresponding pseudo-continuous distribution over appropriate ranges of $\{T_1, T_2\}$. The doped water provided clear confirmation of this relation, Fig. 4(a), where the discrete value of $a_1$ was found to match the distribution integral. It is the integrals of the distribution that are considered useful for petrophysical interpretations, so it is important that similar interpretations can be applied to discrete component fits. For the Ohio Blue sandstone, Fig. 4(b), the smooth inversion delivers a single broad feature where the greedy variational algorithm resolves two distinct components. For the Ketton limestone Fig. 4(c), the multi-modal distribution is resolved into 4 discrete components by our algorithm, and these components visually agree with the smooth peak maxima (see marginal projections). Similarly for the organic shale, Fig. 4(d), the tri-modal

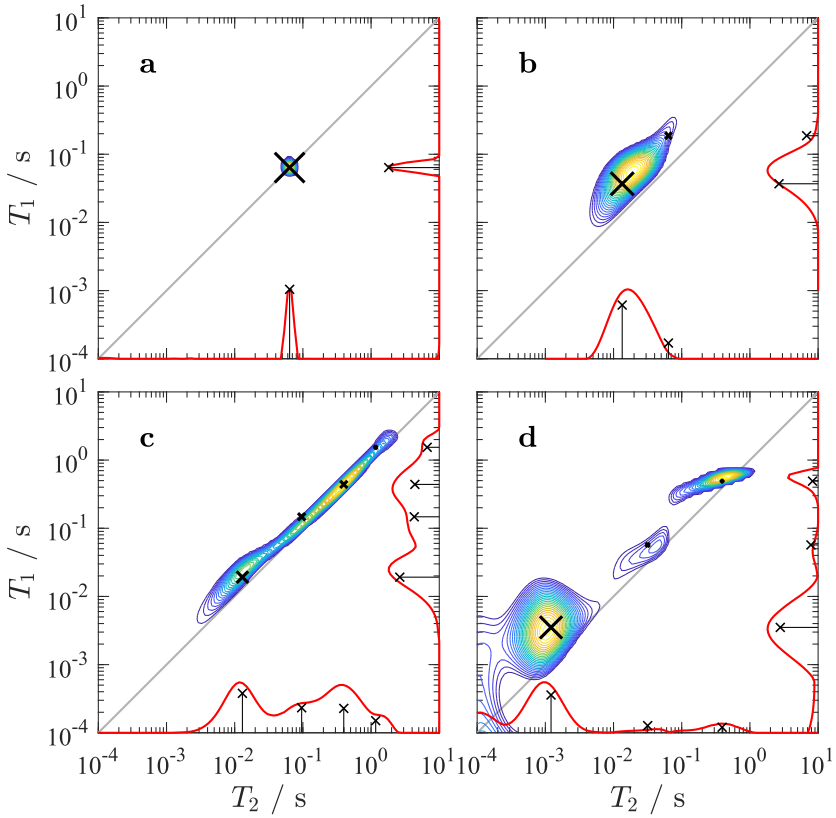


**Fig. 4.** Tikhonov regularization applied to experimental $T_1$-$T_2$ data acquired from (a) doped water, (b) Ohio Blue sandstone, (c) Ketton limestone, and (d) an organic shale. The pseudo-continuous $T_1$-$T_2$ distributions are presented as contour plots with marginal distributions (red lines) included for clarity. The fitted parameter sets $(a_m, T_{1,m}, T_{2,m})$ from Table 2 are overlaid on each main plot (black $\times$ symbols, where the marker size is proportional to $a_m$), with stems in the marginal plots. Fitted components with $T_1/T_2 < 1$ have been omitted. In each plot the diagonal gray line indicates $T_1 = T_2$. (For interpretation of the references to colour in this figure legend, the reader is referred to the web version of this article.)

distribution generated by Tikhonov regularization is reflected in the discrete component fit and, importantly for interpretation of organic shale measurements at low field [34], the correct $T_1/T_2$ ratios are recovered by our greedy variational algorithm.

## 4. Conclusions

We have proposed a new method for approximating $T_1$-$T_2$ distributions from inversion-recovery-CPMG experiments. A greedy variational approach was presented that approximates the usual pseudo-continuous distribution (obtained by Tikhonov regularization, for example) as a sum of discrete Dirac delta functions. The greedy nature of the algorithm promotes sparsity in the solution, leading to a limited number of dictionary elements described by the parameter set $(a_m, T_{1,m}, T_{2,m})$. The variational part of the algorithm estimates these parameters from a continuum at each iteration by reducing the least squares misfit to the data. The computational demand of the variational method depends only on the dictionary size, so the greedy and variational steps are highly complementary. We demonstrated our algorithm in application to synthetic data and experimental measurements of liquid-saturated rock samples. The results were encouraging and agreed with the usual pseudo-continuous distributions generated for petrophysical characterization of reservoir formations. The reduced computational requirement of the greedy variational algorithm and small solution size compared to linear (regularization) inversion methods makes our algorithm a potential candidate for remote or automated NMR measurements, such as logging-while-drilling (LWD) operations, where data bandwidths are limited.

## 5. Experimental method

All NMR data were acquired on an Oxford Instruments GeoSpec system operating at a magnetic field strength of $B_0 = 56$ mT, corresponding to a resonance frequency of $f_0 = 2.4$ MHz for $^1$H. Radio frequency (rf) pulse durations of 15 µs and 30 µs were typical for tip angles of 90° and 180°, respectively. Inversion recovery was performed with wait times incremented logarithmically from $t_W = 1$ ms to 5 s in 32 steps. A single-scan CPMG measurement was performed with an echo time of $t_e = 100$ µs and $K = 20,000$ echoes. A recycle delay of 5 s was allowed between scans and 8 repeat scans were summed to accommodate the phase cycle. Conventional pseudo-continuous $T_1$-$T_2$ correlations were obtained using Tikhonov regularization following the method in [3] with the optimum smoothing parameter selected by generalized cross validation (GCV) [35] as detailed in [36].

Three rock formations, exhibiting a wide variety of relaxation behaviors, were selected for this study: Ohio Blue sandstone, Ketton limestone, and an organic shale. The rock plugs were cored from quarried outcrop blocks. Each plug was a right-cylinder of dimensions 38 mm × 50 mm (diameter × length). The limestone and sandstone plugs were oven dried at 60 °C then vacuum saturated with low salinity brine [37] and wrapped in plastic film for duration of the measurement. The organic shale sample was dried and measured without modification. A bulk reference sample of $NiCl_2$ doped water was also measured.

## Acknowledgments

The authors thank Nick Heaton for helpful discussions.

## References


[1] Y. Song, L. Zielinski, S. Ryu, Two-dimensional NMR of diffusion systems, Phys. Rev. Lett. 100 (2008) 248002.
[2] A.N. Tikhonov, V.Y. Arsenin, Solutions of Ill-posed Problems, V.H. Winston & Sons, Washington D.C., 1977.
[3] L. Venkataramanan, Y.Q. Song, M.D. Hürlimann, Solving Fredholm integrals of the first kind with tensor product structure in 2 and 2.5 dimensions, IEEE Trans. Signal Process. 50 (2002) 1017–1026.
[4] J.P. Butler, J.A. Reeds, S.V. Dawson, Estimating solutions of 1st kind integral-equations with nonnegative constraints and optimal smoothing, SIAM J. Num. Anal. 18 (1981) 381–397.
[5] J.D. Wilson, Statistical approach to the solution of first-kind integral equations arising in the study of materials and their properties, J. Mater. Sci. 27 (1992) 3911–3924.
[6] P.C. Hansen, Discrete Inverse Problems: Insight and Algorithms, SIAM, Philadelphia, 2010.
[7] K.-J. Dunn, D. Bergman, G. LaTorraca, Nuclear Magnetic Resonance - Petrophysical and Logging Applications, Handbook of Geophysical Exploration: Seismic Exploration, Elsevier, 2002.
[8] Y.Q. Song, L. Venkataramanan, M.D. Hürlimann, M. Flaum, P. Frulla, C. Straley, $T_1$-$T_2$ correlation spectra obtained using a fast two-dimensional Laplace inversion, J. Magn. Reson. 154 (2002) 261–268.
[9] M.D. Hürlimann, L. Venkataramanan, C. Flaum, The diffusion-spin relaxation time distribution function as an experimental probe to characterize fluid mixtures in porous media, J. Chem. Phys. 117 (2002) 10223–10232.
[10] R. Kleinberg, H. Vinegar, NMR properties of reservoir fluids, Log Anal. 37 (1996) 20–32.
[11] W. Kenyon, Petrophysical principles of applications of NMR logging, Log Anal. 38 (1997) 21–43.
[12] K.R. Brownstein, C.E. Tarr, Importance of classical diffusion in NMR studies of water in biological cells, Phys. Rev. A 19 (1979) 2446–2453.
[13] S.D. Stoller, W. Happer, F.J. Dyson, Transverse spin relaxation in inhomogeneous magnetic fields, Phys. Rev. A 44 (1991) 7459–7477.
[14] P. Wang, L. Venkataramanan, V. Jain, Sparse clustered bayesian-inspired $T_1$-$T_2$ inversion from borehole NMR measurements, IEEE Trans. Comput. Imag. 3 (2017) 355–368.
[15] M. Fleury, M. Romero-Sarmiento, Characterization of shales using $T_1$-$T_2$ NMR maps, J. Petrol. Sci. Eng. 137 (2016) 55–62.
[16] R. Vold, J. Waugh, M. Klein, D. Phelps, Measurement of spin relaxation in complex systems, J. Chem. Phys. 48 (1968) 3831–3832.
[17] H. Carr, E. Purcell, Effects of diffusion on free precession in NMR experiments, Phys. Rev. 94 (1954) 630–638.
[18] S. Meiboom, D. Gill, Modified spin-echo method for measuring nuclear relaxation times, Rev. Sci. Instrum. 29 (1958) 668–691.
[19] K. Munn, D.M. Smith, A NMR technique for the analysis of pore structure: Numerical inversion of relaxation measurements, J. Colloid Interf. Sci. 119 (1986) 117–126.
[20] A. Reci, A. Sederman, L. Gladden, Obtaining sparse distributions in 2D inverse problems, J. Magn. Reson. 281 (2017) 188–198.
[21] T. Chandrasekera, J. Mitchell, Numerical inversion methods for recovering negative amplitudes in two-dimensional nuclear magnetic resonance relaxation-time correlations, Phys. Rev. E 98 (2018) 043308.
[22] N.H. Williamson, M. Röding, P. Galvosas, S.J. Miklavcic, M. Nydén, Obtaining $T_1$-$T_2$ distribution functions from 1-dimensional $T_1$ and $T_2$ measurements: The pseudo 2-d relaxation model, J. Magn. Reson. 269 (2016) 186–195.
[23] C.E. Yarman, L. Monzón, M. Reynolds, N. Heaton, A new inversion method for nmr signal processing, in: 2013 IEEE 5th International Workshop on Computational Advances in Multi-Sensor Adaptive Processing (CAMSAP), 2013, pp. 260–263.
[24] C.E. Yarman, R. Kumar, J. Rickett, A model-based data-driven dictionary learning for seismic data representation, Geophys. Prospect. 66 (2018) 98–123.
[25] M. Prange, Y.-Q. Song, Quantifying uncertainty in NMR spectra using Monte Carlo inversion, J. Magn. Reson. 196 (2009) 54–60.
[26] R. Salazar-Tio, B. Sun, Monte carlo optimization-inversion method for NMR, Petrophysics 51 (2010) 208–218.
[27] G.E. Hinton, R.R. Salakhutdinov, Reducing the dimensionality of data with neural networks, Science 313 (2006) 504–507.
[28] J. Fan, F. Han, H. Liu, Challenges of big data analysis, National Sci. Rev. (2014) 293–314.
[29] H. Grage, M. Akke, A statistical analysis of NMR spectrometer noise, J. Magnet. Reson. 162 (2003) 176–188.
[30] J. Nocedal, S.J. Wright, Numerical Optimization, second ed., Springer, New York, 1999.
[31] G. Golub, V. Pereyra, Separable nonlinear least squares: the variable projection method and its applications, Inv. Prob. 19 (2003) R1.
[32] R. Kleinberg, S. Farooqui, M. Horsfield, $T_1/T_2$ ratio and frequency dependence of NMR relaxation in porous sedimentary rocks, J. Colloid Interf. Sci. 158 (1993) 195–198.
[33] M. Hürlimann, D. Griffin, Spin dynamics of Carr-Purcell-Meiboom-Gill-like sequences in grossly inhomogeneous $B_0$ and $B_1$ fields and application to NMR well logging, J. Magn. Reson. 143 (2000) 120–135.
[34] R. Kausik, K. Fellah, E. Rylander, P. Singer, R. Lewis, S. Sinclair, NMR relaxometry in shale and implications for logging, Paper presented at the SPWLA 56th Annual Logging Symposium, July 18-22, 2015.
[35] G. Wahba, Practical approximate solutions to linear operator equations when data are noisy, SIAM J. Numer. Anal. 14 (1977) 651–667.
[36] J. Mitchell, T. Chandrasekera, L. Gladden, Numerical estimation of relaxation and diffusion distributions in two dimensions, Prog. Nucl. Magn. Reson. Spectrosc. 62 (2012) 34–50.
[37] J. Mitchell, J. Staniland, R. Chassagne, E. Fordham, Quantitative in situ enhanced oil recovery monitoring using nuclear magnetic resonance, Transp. Porous Med. 94 (2012) 683–706.